catalysts

MDPI

Article

Facile Fabrication of SiO_2/Zr Assisted with EDTA Complexed-Impregnation and Templated Methods for Crude Palm Oil to Biofuels Conversion via Catalytic Hydrocracking

Hasanudin Hasanudin [1,2,*], Wan Ryan Asri [1,2], Zainal Fanani [1,2], Selvi Julpani Adisti [1,2], Fitri Hadiah [3], Roni Maryana [4], Muhammad Al Muttaqii [4], Zongyuan Zhu [5] and Nelio Teixeira Machado [6]

[1] Department of Chemistry, Faculty of Mathematics and Natural Science, Universitas Sriwijaya, Inderalaya 30662, South Sumatra, Indonesia
[2] Biofuel Research Group, Faculty of Mathematics and Natural Science, Universitas Sriwijaya, Inderalaya 30662, South Sumatra, Indonesia
[3] Department of Chemical Engineering, Faculty of Engineering, Universitas Sriwijaya, Inderalaya 30662, South Sumatra, Indonesia
[4] Research Center for Chemistry, Indonesian Institute of Sciences, Building 452 Kawasan PUSPIPTEK, Serpong, Tangerang Selatan 15311, Banten, Indonesia
[5] School of Energy and Power, Jiangsu University of Science and Technology, Zhenjiang 212000, China
[6] Faculty of Sanitary and Environmental Engineering, Campus Profissional-UFPA, 17 Universidade Federal do Pará, Rua Corrêa N° 1, Belém 66075-900, Brazil
* Correspondence: hasanudin@mipa.unsri.ac.id

Citation: Hasanudin, H.; Asri, W.R.; Fanani, Z.; Adisti, S.J.; Hadiah, F.; Maryana, R.; Al Muttaqii, M.; Zhu, Z.; Machado, N.T. Facile Fabrication of SiO_2/Zr Assisted with EDTA Complexed-Impregnation and Templated Methods for Crude Palm Oil to Biofuels Conversion via Catalytic Hydrocracking. *Catalysts* **2022**, *12*, 1522. https://doi.org/10.3390/catal12121522

Academic Editor: S. David Jackson

Received: 19 October 2022
Accepted: 21 November 2022
Published: 25 November 2022

Publisher's Note: MDPI stays neutral with regard to jurisdictional claims in published maps and institutional affiliations.

Abstract: Zr-containing SiO_2 and their parent catalysts were fabricated with different methods using EDTA chelation and template-assist. The activity of the catalysts was explored in crude palm oil (CPO) hydrocracking, conducted under a continuous system micro-cylindrical reactor. The conversion features and the selectivity towards biofuel products were also examined. The physicochemical of catalysts, such as structure phase, functional groups, surface morphologies, acidity features, and particle size, were investigated. The study showed that the template method promoted the crystalline porous catalysts, whereas the chelate method initiated the non-porous structure. The catalysts' acidity features of SiO_2 and SiO_2/Zr were affected by the preparation, which revealed that the EDTA chelate-assisted method provided higher acidity features compared with the template method. The CPO hydrocracking study showed that the SiO_2/Zr-CEDTA provided the highest catalytic activity towards the hydrocracking process, with 87.37% of conversion attained with 66.29%.wt of liquid product. This catalyst exhibited selectivity towards bio-jet (36.88%), bio-diesel (31.43%), and bio-gasoline (26.80%). The reusability study revealed that the SiO_2/Zr-CEDTA had better stability towards CPO conversion compared with SiO_2/Zr-CEDTA, with a low decrease in catalyst performance at three consecutive runs.

Keywords: EDTA; SiO_2; SiO_2/Zr; crude palm oil; hydrocracking; biofuel

1. Introduction

The availability of sustainable and clean energy is currently a considerable concern [1]. The dominant conventional energy source is gradually utilized over time, resulting in a deracination of the fuel supply [2,3]. Furthermore, the emission of greenhouse gases, such as CO_x, SO_x, NO_x, and other poisonous gases from the exhaustion of conventional fuels, is a critical concern because it is counterproductive to human health and the environment [4]. Amidst this obstacle, the courageous concept of developing alternative energy sources, such as biofuels, bravely emerged [5]. Biofuels are known to be renewable, eco-friendly, and sustainable, and designate their potential for substitution while

reducing reliance on fossil fuels [6,7]. Depending on the number of carbon atoms, these fuels are classified into numerous fractions, such as gasoline, kerosene, and diesel [8].

Methods regarding the production of biofuels have been explored extensively. Among the methods that have been employed, the catalytic cracking and hydrocracking methods seem to be the preferred processes as they produce a wide range of hydrocarbons, with particular boiling points that may be directly applied as fuels [9]. This technology offers several advantages, including a lower operating temperature than the pyrolysis method, a more straightforward operating route, and a high conversion feature, with a high calorific value and oxygen-free output [10–12]. In this operation, the double bonds in triglycerides as raw material are cracked down into smaller compound hydrocarbon molecules in the presence of hydrogen and a coherently suitable catalyst [13].

The feedstock of the catalytic hydrocracking reaction is an essential consideration in the production of biofuels. Numerous triglycerides feedstocks, such as algae oil, nyamplung oil, palm oil, soybean, safflower, jatropha, and soybean, have been progressively utilized in the hydrocracking process [6,14–19]. Specifically, the use of crude palm oil (CPO) as a biofuel feedstock is propitious, considering the massive production previously reported [20]. CPO has an extortionate yield per hectare compared to other vegetable oils [21]. For instance, Indonesia has 14 million hectares of oil palm and delivers 85% of the world's palm oil [22]. CPO has a high hydrocarbon chain content with nitrogen and sulfur-free, respectively [23,24]. Considering its chemical nature, readily abundance, and especially its contribution to the Indonesian economy, CPO as a feedstock for producing biofuels via catalytic hydrocracking is reasonably profitable and sustainable.

The development of sufficient catalysts for the vegetable oils' catalytic hydrocracking into biofuels is an essential thing and one of the critical parameters. Among the available catalysts, SiO_2 is one of the catalysts that has enchanted attention due to its high thermal/hydrothermal stability, which results in adequate selectivity for biofuel products and encourages increased oil yields [25]. SiO_2 has been widely expanded due to its chemical stability, vast surface area, non-toxicity, relatively inexpensive, and eco-friendly [26].

In recent decades, metal-support catalytic systems have been explored due to their resistance to catalyst poisoning and deactivation. Currently, SiO_2 has been used as a supported catalyst in many active species such as Ni-Zr [27], Cu [28,29], Ni [30,31], ZnO [32], Ag_2O, Na_2O and K_2O [33], NiP [34], CrO_x [35], and Ru [36]. In particular, active zirconia-based-catalysts have fascinated researchers, in which exhibiting Lewis acid behavior and high catalytic features have been recognized as relatively inexpensive, low toxicity, green, and efficient catalysts for various major organic transformations [37]. Zirconia has both acidic and metallic features, high surface area, remarkable chemical stability, and exceptional surface chemical activity, which can be exploited for the enhancement of oxygen-containing chemicals such as vegetable oil [38]. Zhao et al. [39] adapts the silica with zirconium sites to produce a material with well-defined features. The study report that the hydrogenation catalytic activity and selectivity features were remarkably enhanced by the Zr modification of the silica support compared to Co/SiO_2. Therefore, there is a reasonable impulsion for SiO_2/Zr to explore their potential as an effective cracking reaction catalyst.

Nowadays, the modulation of the physicochemical properties of the catalyst can be conducted by various approaches. The use of chelating agents [40–45] and templates [46–48] has recently captivated attention because they can modify or tune the catalyst's surface, structural, and textural properties, depending on the purpose of the application. Many complexing agents have been employed to enhance the physicochemical properties of various types of catalysts, including citric acid [40–42], L-arginine [43], EDTA-citric acid [44], glycinate [45], ethylene diamine and acetic acid [40]. The effects of these chelating compounds on the catalysts Ni/SBA-16, Ni/ZrO_2, mesoporous Sm/Ce, Ni/SiO_2, Ni/-alumina, and Ni/SBA-15 have all been investigated. Notably, the use of EDTA chelating agent has been reported considerably improved the Co/SiO_2 nano spring catalyst as well as their catalytic activity on Fischer-Tropsch CO hydrogenation and catalyst selectivity. This chelating agent's ability to promote Co_3O_4 dispersion on the support surface has been

investigated [49]. The modification of SiO_2/Zr using several techniques, such as templating and chelating methods, and comparing their respective effects on the catalytic activity of hydrocracking, have not been studied yet. Furthermore, neither exploration nor report has been made for fabricating the SiO_2/Zr using an EDTA species as chelating and templating agents. Within this frame of reference, the use of EDTA has the potential as a SiO_2 template or chelating agent, considering that these species are capable of complex binding to zirconium, and calcination at high temperatures will cause EDTA to be removed, allowing changes in the physicochemical properties of SiO_2/Zr.

This work presents a simple facile route for the synthesis of SiO_2/Zr through the complexed-impregnation method. The effect of EDTA as a chelating agent and template method on the physicochemical features of Zr/SiO_2 will be explored and assessed using multiple characterization techniques such as PSA, SEM-EDS mapping, N_2 physorption, XRD, FTIR, FTIR-absorbed pyridine, as well as the total and the surface acidity features using the gravimetric method. The catalytic activity of these as-prepared catalysts will be examined through the catalytic hydrocracking of CPO toward biofuels.

2. Results and Discussion

2.1. Characterization of Catalysts

A series of SiO_2, SiO_2/Zr catalysts, and their counterparts were prepared using different methods by employing an EDTA template and chelate agents. Their physicochemical properties were assessed using various characterizations. Figure 1 represented the diffractograms of SiO_2, SiO_2/Zr, and their modification using EDTA as a template and chelate as well. The SiO_2 diffractogram revealed a broad peak at 23°, which was assigned to the amorphous silica (ICDD No. 39-1425) [50]. Another study also observed this typical peak when preparing SiO_2 using the sol-gel method [51]. Notably, the 2θ peaks at 30.11°, 34.76°, 50.30°, and 60.10° which was attributed to the single tetragonal zirconia phase (ICDD No. 80-2155) [52]. Some studies reported that the zirconia also had monoclinic, cubic, and mixed crystal structure phases [53,54], which depend on the catalyst's preparation. The amorphous silica phase was still presented on SiO_2/Zr, which indicated that the amorphous silica structure was preserved [55].

As seen in Figure 1, the EDTA chelate and template-assisted method promoted a significantly different crystal structure towards SiO_2/Zr. These results indicate that the EDTA species employed with different methods, i.e., chelate and template, positively affected the SiO_2/Zr structure. The SiO_2/Zr-CEDTA revealed an amorphous structure with no zirconia phase were discerned, which suggested that the Zr species was finely dispersed towards the silica surface and relatively diminutive to be identified by the XRD [40]. This result was also reported by Nadia et al. [56] when preparing NiMo/silica induced by different species such as $NaHCO_3$, whereby the Mo species was not distinguishable after being loaded onto silica. Rubab et al. [48] reported that there was no discernible crystal structure in SiO_2/NiO, which might be attributed to the integration of NiO into the SiO_2 matrix, as well as its amorphous nature and slighter crystallite size. This result also suggests that the EDTA chelate-assisted method was changing the tetragonal phase zirconia to the amorphous structure, which was presumably due to the robust bonded interaction between the EDTA and Zr through the complex bond, thus leading to the inefficient Zr crystallization. By contrast, the SiO_2 prepared by the EDTA template-assisted method (SiO_2-TEDTA) enhanced the silica structure to be crystalline, as indicated, and new peaks were formed, which attributed to the mixed phase, such as quartz (ICDD No. 71-5334) and cristobalite (ICDD No. 89-3606). During the calcination process, the EDTA species was removed and presumably generated highly ordered silica, thus leading to crystalline phase structure. Similarly, the SiO_2/Zr prepared by the template-assisted method was also appeared a crystalline structure. Moreover, the additional peaks at 26.76° in SiO_2/Zr-TEDTA suggested the presence of a monoclinic zirconia phase [52], whereas the unobservable, other monoclinic phase presumably due to the overlapping peaks between

crystalline silica. The relative shift of the tetragonal zirconia phase occurred, likely due to the effect of EDTA species as a templating agent.

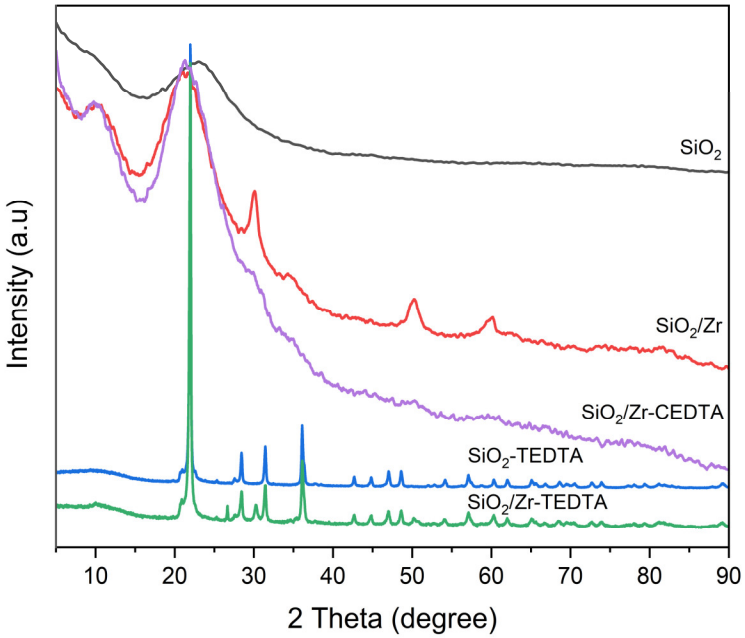

Figure 1. XRD diffraction of SiO_2, SiO_2/Zr, SiO_2/Zr-CEDTA, SiO_2-TEDTA, and SiO_2/Zr-TEDTA.

The FTIR spectra of SiO_2, SiO_2/Zr, and their modification are depicted in Figure 2. The absorption band at 1003 and 890 cm^{-1} on the SiO_2 catalyst (Figure 2a) were attributed to the asymmetric and symmetric Si-O stretching vibration [57], whereas the bending mode of Si-O-Si and O-Si-O bonds were observed at 738 and 421 cm^{-1}, respectively [58]. These peaks also appeared in SiO_2 prepared by the EDTA template (Figure 2c) with a relatively shifted towards the lower wavelength, which suggested the local bonding structure change of O and Si atoms promoted by the EDTA template. Meanwhile, the silanol absorption bands were relatively unobserved on the SiO_2/Zr catalyst (Figure 2b), which was presumably due to the intensive band of silanol groups, thus overlapping the zirconia groups bands.

As shown in Figure 2, since catalysts involved the same functional groups, there was no appreciable peak change of SiO_2/Zr prepared by the chelate method compared with the parent SiO_2/Zr, whereas there was a slightly different absorption band at a low wavelength when the template method was employed. This condition suggested that the template and chelate methods affected how the functional groups of silanol as well as zirconia groups bonded in the SiO_2/Zr catalyst. The absorption band at 3650 cm^{-1} and 1556 cm^{-1} corresponded to the Si-OH and -OH groups, respectively [55,59], which were maintained for all catalysts.

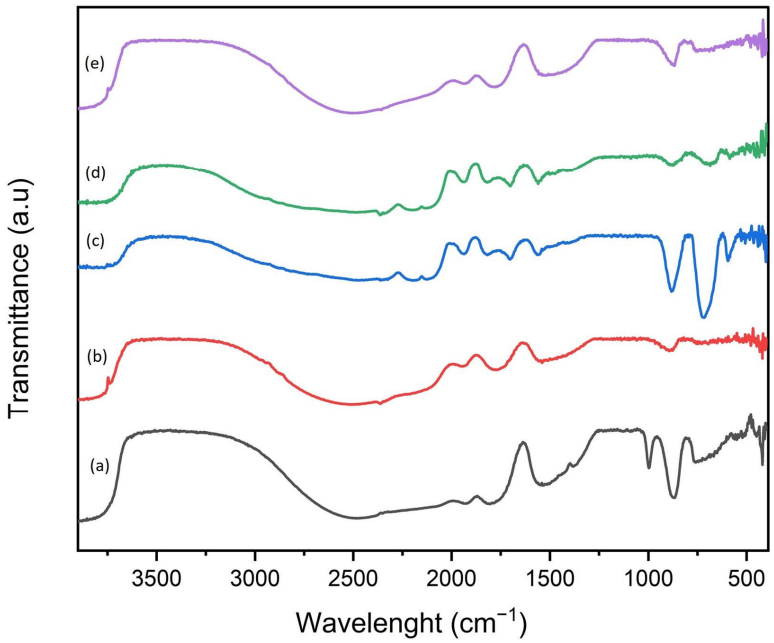

Figure 2. FTIR spectra of (a) SiO_2 (b) SiO_2/Zr (c) SiO_2-TEDTA (d) SiO_2/Zr-TEDTA and (e) SiO_2/Zr-CEDTA.

The SEM micrographs of modified SiO_2, SiO_2/Zr, and their parent catalysts are presented in Figure 3. SiO_2 catalyst (Figure 3a) had a tiny particle distributed uniformly, and after being loaded by the Zr species (Figure 3b), the agglomerated silica was formed which acted as the support for the Zr species.

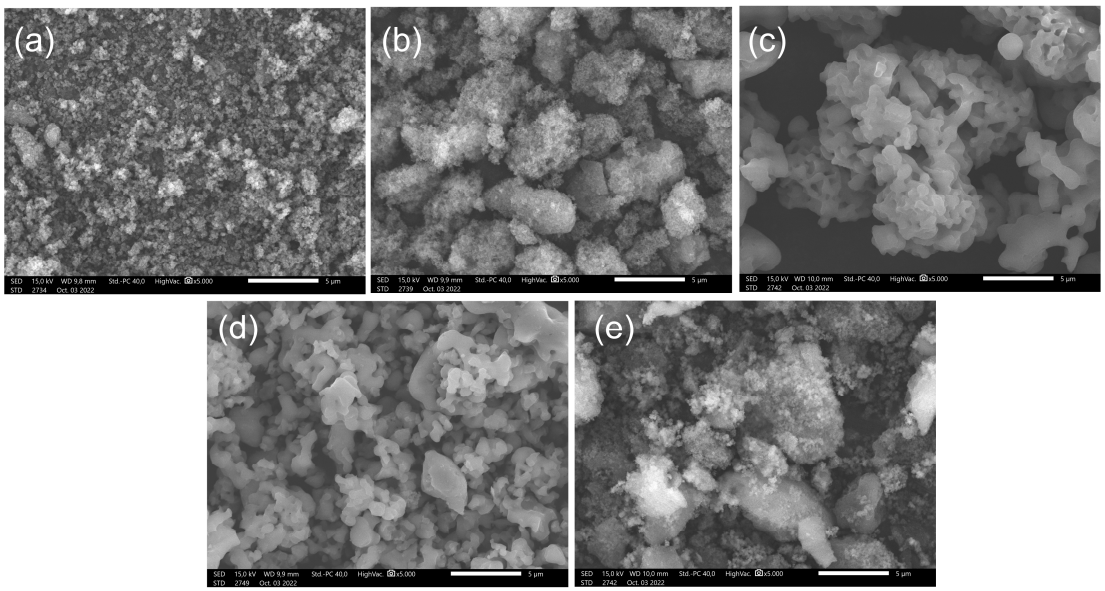

Figure 3. SEM micrographs of (**a**) SiO_2 (**b**) SiO_2/Zr (**c**) SiO_2-TEDTA (**d**) SiO_2/Zr-TEDTA and (**e**) SiO_2/Zr-CEDTA.

Remarkably, the SiO_2/Zr prepared by the EDTA template method (Figure 3c) displayed a high porous structure allocated uniformly, the same as the SiO_2/Zr-TEDTA (Figure 3d) but with a less uniformly expanded porous structure. Meanwhile, the SiO_2/Zr prepared by the EDTA chelate method revealed an uneven non-porous structure. These

results suggested that the EDTA template-assisted method promoted the crystalline porous structure, whereas the EDTA chelate-assisted method led to the non-porous and amorphous structure.

The EDX mapping of all catalysts is presented in Figure 4. The expected elements of all catalysts, such as Si, O, and Zr, exist in Figure 4a–e. It can be seen that there was an adequate homogenous zirconium species dispersion towards the surface of the SiO_2, which could promote the metal-support interaction [60]. However, the distribution of SiO_2 as catalyst support was displayed differently depending on their preparation, which suggested that the EDTA chelate and template method positively affected the catalysts' morphological surface by promoting the enhancement of Zr dispersion.

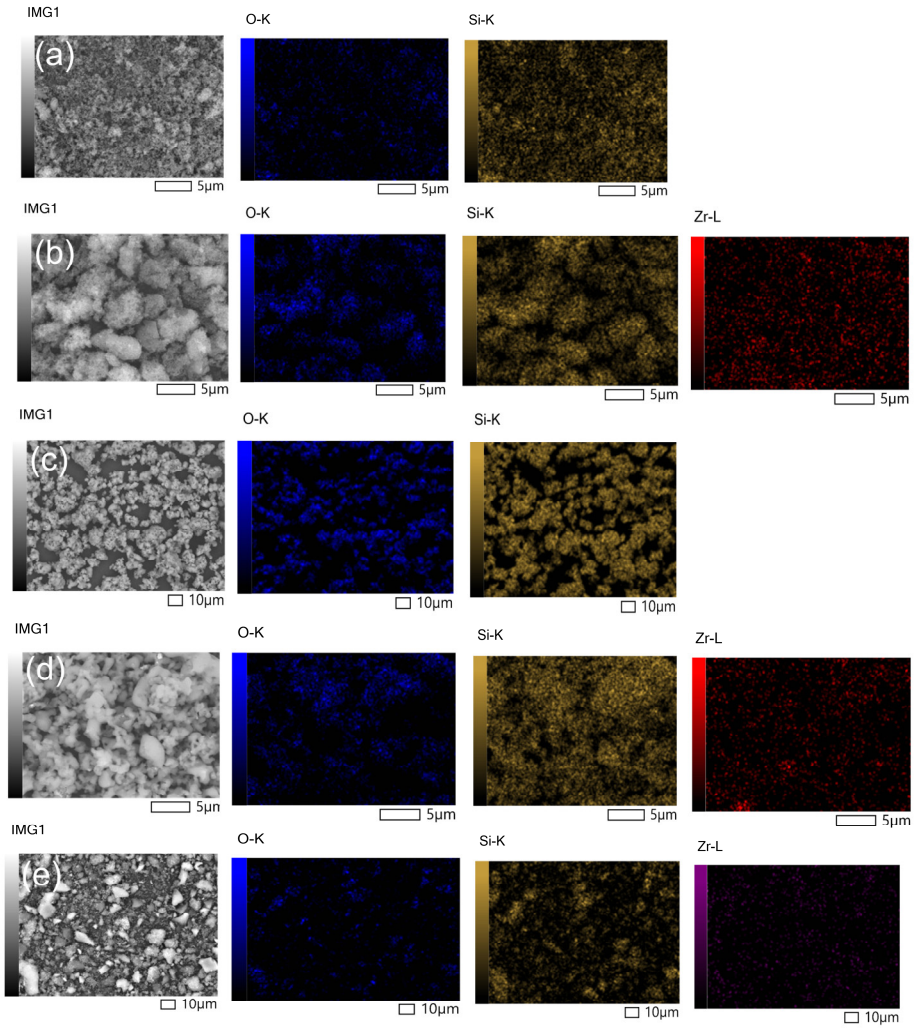

Figure 4. EDX mapping of (**a**) SiO_2 (**b**) SiO_2/Zr (**c**) SiO_2-TEDTA (**d**) SiO_2/Zr-TEDTA and (**e**) SiO_2/Zr-CEDTA.

The EDX elemental analysis is shown in Table 1. It can be seen that the Zr content was presented correspondingly over SiO_2/Zr, and their counterparts, with no impurities. These results suggested that the SiO_2/Zr catalysts were successfully prepared.

Table 1. EDX results of SiO_2, SiO_2/Zr, and their modification.

Catalyst	Atomic (wt.%)		
	Si	O	Zr
SiO_2	18.68	81.33	
SiO_2/Zr	21.6	78.14	0.26
SiO_2-TEDTA	28.43	71.57	
SiO_2/Zr-TEDTA	26.18	73.43	0.39
SiO_2/Zr-CEDTA	21.6	77.85	0.55

The N_2 physisorption of SiO_2, SiO_2/Zr, and their modification using chelate and template methods are presented in Figure 5. Based on the IUPAC categorization, it was apparent that all the catalysts had a type IV isotherm with a hysteresis loop of type H4, which suggested that the catalysts were mesoporous. Furthermore, the H4 hysteresis loop was related to the micropores with narrow slits feature [56].

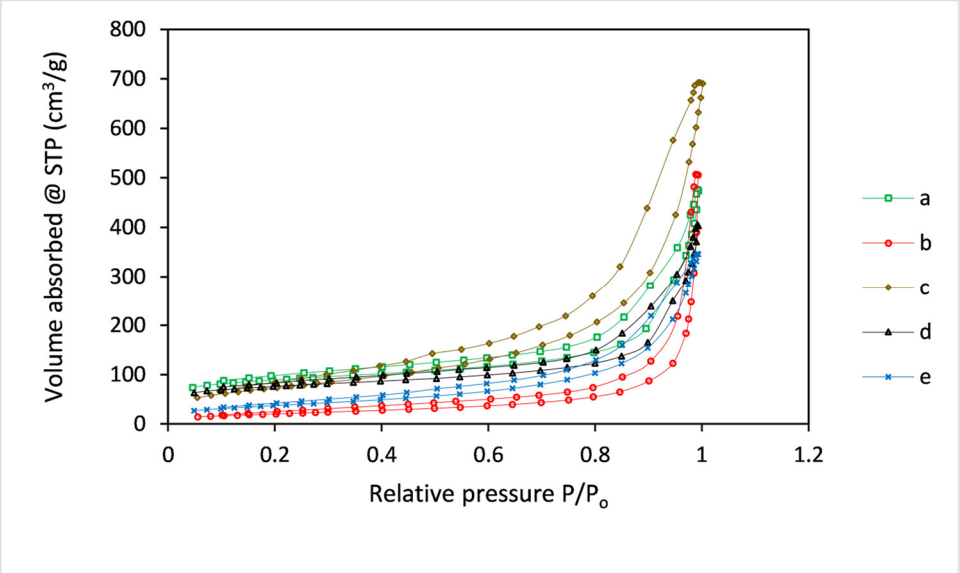

Figure 5. N_2 physorptions of (a) SiO_2 (b) SiO_2/Zr (c) SiO_2-TEDTA (d) SiO_2/Zr-TEDTA (e) SiO_2/Zr-CEDTA.

The textural features of all catalysts are shown in Table 2. The surface area of SiO_2 significantly decreased after being loaded by the Zr species, presumably due to the pore blocking of Zr species [61]. It can be seen that the SiO_2/Zr-KEDTA and SiO_2/Zr-CEDTA had higher surface area compared with the parent SiO_2/Zr catalyst, whereas the SiO_2 prepared by the template method relatively decreased the surface area of the catalyst but increased the total pore volume as well as the average pore radius of the catalysts. This condition indicated that the template and chelate method affected the textural properties of catalysts. The porous structure generated by the EDTA template method enhanced the pore volume of catalysts, whereas the EDTA chelate method reduced the total pore volume of SiO_2/Zr-CEDTA.

Table 2. Textural features of catalysts.

Catalyst	Surface Area (m^2/g)	Total Pore Volume (cm^3/g)	Average Pore Radius (Å)
SIO_2	294	0.73	49.76
SIO_2/Zr	76.43	0.78	20.48
SIO_2-TEDTA	268	0.81	60.44
SIO_2/Zr-TEDTA	220.5	0.83	75.37
SIO_2/Zr-CEDTA	134	0.53	79.58

The average particle size distribution of all catalysts is presented in Figure 6. It can be seen that the SiO_2 catalyst (Figure 6a) had a relatively uniform particle distribution and subsequently led to a non-uniform particle size distribution after being loaded by the Zr species (Figure 6b). SiO_2-TEDTA catalyst (Figure 6c) had narrow particle size distribution with better uniformity compared with SiO_2. In contrast, surprising results were obtained on the SiO_2/Zr catalyst, both prepared using the template and the chelate methods (Figure 6c,d), as it revealed a non-uniform particle size distribution. However, SiO_2/Zr-CEDTA showed a higher non-uniform particle size distribution than SiO_2/Zr-TEDTA.

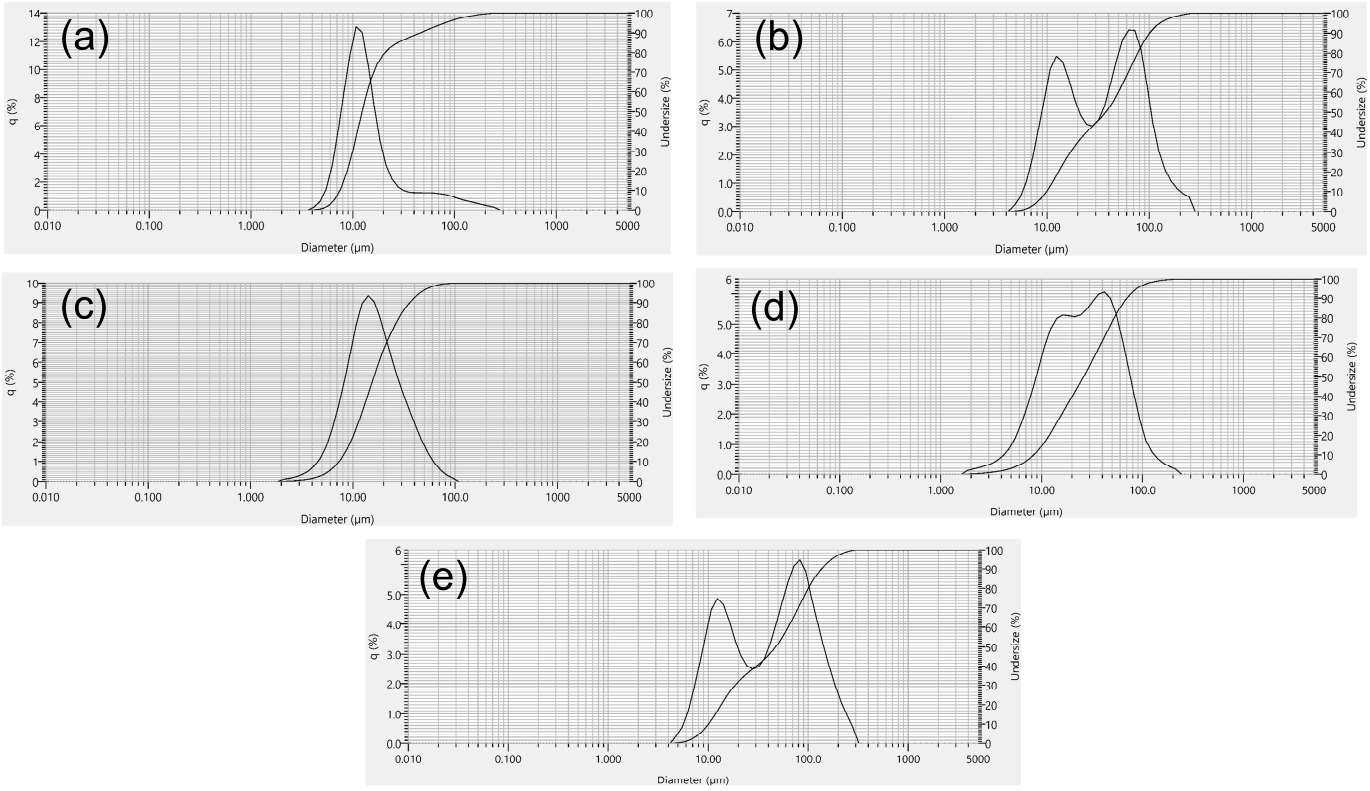

Figure 6. Particle size distribution of (**a**) SiO_2 (**b**) SiO_2/Zr (**c**) SiO_2-TEDTA (**d**) SiO_2/Zr-TEDTA and (**e**) SiO_2/Zr-CEDTA.

The average particle size of all catalysts is presented in Table 3. It can be seen that the average particle size of SiO_2/Zr was higher than the parent SiO_2, presumably due to the effect of Zr impregnation towards the SiO_2 catalyst, which generated aggregate particles. By employing the EDTA template method, the average particle size of SiO_2 tended to decrease, likely due to the porous structure formation, which reduced the average particle size. Regarding SiO_2/Zr catalyst, similarly, employing the template method decreased the average particle size of the catalyst, whereas the chelate method promoted conversely. The strong interaction of metal species with the EDTA through the chelate method likely

provided a dense structure, thus leading to the increase in the catalyst's average particle size.

Table 3. Average particle size (μm) of SiO_2, SiO_2/Zr, and their modification.

Catalyst	Average Particle Size (μm)
SiO_2	21.66 ± 0.32
SiO_2/Zr	48.39 ± 0.05
SiO_2-TEDTA	19.08 ± 0.07
SiO_2/Zr-TEDTA	34.26 ± 0.16
SiO_2/Zr-CEDTA	61.45 ± 0.07

The total, surface, and pore acidity of all catalysts are presented in Figure 7. It was distinctly seen that the SiO_2 had a low acidity feature when compared to SiO_2/Zr. This low acidity feature was correlated to the Si^{4+} ions, which acted as Lewis acid sites [55], and gradually increased due to the existence of Zr species that contribute to the increase in SiO_2 acidity [62]. The catalyst prepared by the template method seemed to decrease the catalysts' acidity features for both SiO_2 and SiO_2/Zr, whereas SiO_2/Zr prepared by the chelate method promoted an increase in total and surface acidity as well. The low acidity of SiO_2-TEDTA and SiO_2/Zr-TEDTA was presumably due to the porous structure of the catalyst. The interrelatedness of many active sites on the catalyst surface with one another could happen, thus leading to overlapping between active groups in the catalyst, thereby prompting non-optimal probe absorption [63]. It also can be seen from Figure 7 that the active catalyst site of SiO_2 and SiO_2/Zr was likely generated from the catalysts' pores rather than the surface, whereas the catalyst prepared by the chelate method enhanced the catalyst acidity surface, which consequently decreased the pore acidity. This condition suggested that the template and chelate methods generated different acidity features of the prepared catalyst.

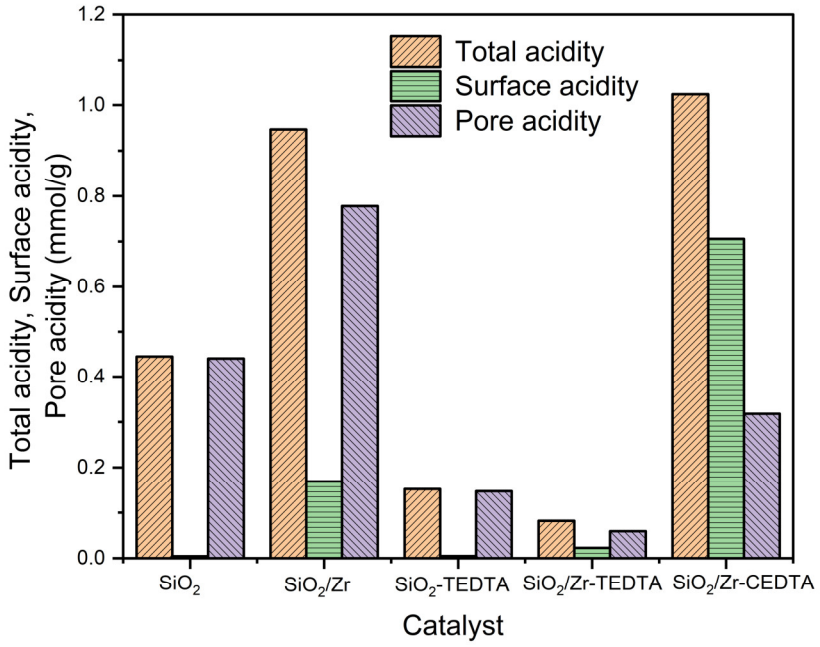

Figure 7. Total, surface, and pore acidity of the catalyst.

The FTIR-pyridine absorbed of SiO_2/Zr and their modification is presented in Figure 8. It can be seen that the intensity of SiO_2/Zr and SiO_2/Zr-CEDTA at specific

wavelengths were increased after pyridine was absorbed, whereas SiO_2/Zr-TEDTA showed no appreciable intensity change, which is consistent with the gravimetric analysis, as reported earlier. The broad absorption band at ca. 1630 cm^{-1} was attributed to the Bronsted acid site initiated by the pyridinium ion [12], whereas the Lewis acid site was observed at ca. 1450 cm^{-1} absorption band [56]. The strong intensity of the Lewis acid site was noticed on the SiO_2/Zr-CEDTA, suggesting that the chelate method promoted a high catalyst acidity.

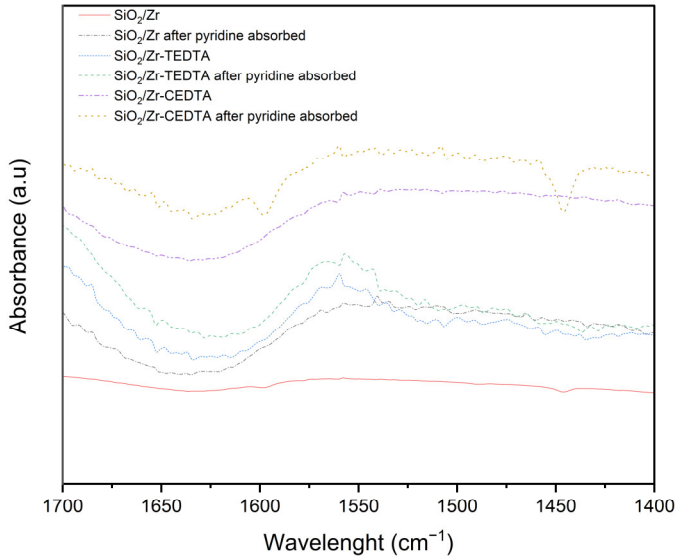

Figure 8. FTIR spectra of SiO_2/Zr, SiO_2/Zr-TEDTA, and SiO_2/Zr-CEDTA before and after pyridine adsorption.

2.2. Hydrocracking Test

The catalytic activity of all catalysts was evaluated for CPO hydrocracking by using a catalyst weight of 0.5 g, a hydrogen flow rate of 30 mL/min, a feed flow rate of 20 mL/h, and a hydrocracking temperature of 500 °C for 1 hr. The conversion and product yield of the hydrocracking process are presented in Table 4.

Table 4. Conversion and product yield from CPO hydrocracking with various catalysts.

Catalyst	Conversion (%)	Yield (%.wt)			
		Liquid	Gas	Coke	Residue
SiO_2	77.10	53.44	17.971	0.09	28.58
SIO_2/Zr	82.75	45.93	40.23	0.21	13.63
SIO_2-TEDTA	60.33	62.84	12.99	0.02	24.15
SIO_2/Zr-TEDTA	62.17	47.45	38.43	0.12	14
SIO_2/Zr-CEDTA	87.73	66.29	23.33	0.34	10.04

It can be seen that the SiO_2/Zr generated a much higher conversion compared to SiO_2. The presence of Lewis acid from Zr species presumably promoted the increase of hydrocracking conversion. Similar findings were also reported by Alisha et al. [64], which showed that the addition of metal species on the support (Mo/SBA-15) promoted the conversion of waste palm cooking oil to hydrocarbon. The low conversion of triglycerides through the hydrocracking process catalyzed by silica was also reported by other studies [55]. Meanwhile, the catalyst prepared by the EDTA template method likely decreases the

conversion of both, SiO_2 and SiO_2/Zr catalysts. On the contrary, SiO_2/Zr prepared by the chelate method promoted high conversion up to 87.73%. These results indicated that the acidity of the catalyst affected the hydrocracking conversion, whereby the chelate method preparation promoted the synergetic effect towards high conversion. Based on Table 3, all catalysts relatively generated high yields due to high-temperature hydrocracking. The SiO_2/Zr had the lowest liquid yield with high gas yield compared with other catalysts. The high gas produced over the SiO_2/Zr catalyst was presumably due to high pore acidity, which promoted the excessive hydrocracking process, thereby increasing the gas yield. The gas product commonly consists of the uncondensable gas such as CO, CO_2, and other C_1-C_5 hydrocarbons. It seemed that the SiO_2/Zr prepared by the template and chelate method higher the liquid yield and reduced the gas yield as well, with pronounced activity observed by the SiO_2/Zr -CEDTA catalyst. Similarly, the SiO_2-TEDTA had a higher liquid yield compared with the parent SiO_2. The porous structure of the catalyst prepared by this method assumably promoted the high liquid yield rather than its acidity. According to these results, the SIO_2/Zr-CEDTA generated the highest liquid compared with another catalyst. SiO_2 catalyst had low coke due to the low acidity of the catalyst, whereas the SiO_2/Zr-CEDTA generated high coke yield compared with others. Wijaya et al. [55] stated that high catalyst acidity could induce coke formation. Based on Table 4, the residue yield of the hydrocracking process for all catalysts ranges from 10.04–28.58%. The residue product consists of the unreacted triglyceride, and the lowest residue yield (10.04%) was achieved by the SIO_2/Zr-CEDTA, which suggested that the SIO_2/Zr prepared by the chelate method was the most effective for CPO hydrocracking compared with other prepared catalysts.

Table 5 shows the selectivity product towards bio-gasoline and bio-aviation with different catalysts. It can be seen that the SiO_2 catalyst provided high selectivity towards the bio-diesel product, with the lowest bio-gasoline fraction. The lowest bio-gasoline fraction was generated, presumably due to low catalyst acidity [55]. Compared with the parent SiO_2, the SiO_2/Zr catalyst increased the bio-gasoline and bio-jet selectivity and decreased the bio-diesel selectivity. Furthermore, the bio-jet selectivity increased after the SiO_2 catalyst was prepared by the template method. This condition suggested that the porous structure of SiO_2-TEDTA provided effective diffusion towards the bio-jet product. During the CPO hydrocracking process, triglycerides and hydrogen gas diffused to the surface or pores of the catalyst and were followed by adsorption to the active site of the catalyst. This step would crack the triglycerides into carbon atoms with lower chains forming the biofuel fraction and some gases. After that, the product was desorbed from the surface of the catalyst and subjected to diffusion into the gas phase. Meanwhile, the selectivity of bio-jet, as well as bio-diesel, is relatively the same when employing the SiO_2/Zr-TEDTA catalyst. Moreover, the SiO_2/Zr prepared by the template and chelate method generated no significant change in the bio-gasoline selectivity.

Table 5. Biofuel product selectivity from CPO hydrocracking over various catalysts.

Catalyst	Selectivity (%)		
	Bio-gasoline	**Bio-jet**	**Bio-diesel**
SiO_2	23.13	31.64	45.23
SiO_2/Zr	24.58	34.47	40.95
SiO_2-TEDTA	27.23	44.67	28.1
SiO_2/Zr-TEDTA	26.94	36.88	36.18
SiO_2/Zr-CEDTA	26.80	41.77	31.43

The reusability study of catalysts was evaluated to understand the catalyst's stability towards CPO conversion. Table 6 compares the reusability performance of SiO_2/Zr-TEDTA and SiO_2/Zr-CEDTA toward CPO conversion. As can be seen in Table 2, the catalytic performance of SiO_2/Zr-TEDA after the second run decreased up to 8.73%, and

continually decreased up to 21.28% compared with the first run. Meanwhile, only 11.79% of the decrease in catalytic performance was observed when employing the SiO_2/Zr-KEDTA, which suggested that the chelate method provides a relatively stable conversion towards CPO. The decrease in the conversion during the consecutive run was presumably due to coke deposition [7]. It has been known that the catalyst could deactivate through coke formation. This coke blocked the catalyst's active site to initiate the reaction, thereby reducing the catalyst's performance [62].

Table 6. Reusability study of SiO_2/Zr-TEDTA and SiO_2/Zr-CEDTA catalysts.

Catalyst	Conversion (%)		
	1st run	2nd run	3rd run
SiO_2/Zr-TEDTA	61.25	56.12	48.21
SiO_2/Zr-CEDTA	85.63	82.23	75.53

3. Materials and Methods

3.1. Preparation of SiO_2/Zr Using EDTA Template-Assisted

All chemicals are earned from Merck and utilized without purification. In this typical procedure, tetraethyl orthosilicate (25 mL) was mixed with ethanol (50 mL) and stirred for 15 min at RT. Afterward, sodium ethylenediaminetetraacetic solution (10%, 20 mL) was added, and the ammonium hydroxide solution was gradually dripped (28%, 2 mL) and stirred for 3 hrs. The gel was left at RT for 30 min and subsequently dried in the oven at 85 °C for 24 hrs. The dried powder was later calcined in the muffle furnace at 850 °C for 3 hrs. under an oxygen atmosphere (30 mL/h). The as-prepared catalyst was denoted as SiO_2-TEDTA. The SiO_2-TEDTA was repeatedly washed with deionized water through centrifugation (3500 rpm) for 10 min until the pH reached 7. The solution was later heated to evaporate the water and subsequently dried at 120 °C for 24 hrs. Finally, the dried SiO_2-EDTA powder was mixed with the $ZrOCl_2.8H_2O$ solution (200 mL, 0.04 mol/L) and stirred for 1 hr. at RT. The temperature was gradually increased up to 80 °C for 3 hrs. The paste was dried at 120 °C for 3 hrs. and was later calcined at 850 °C for 3 hrs. under an oxygen atmosphere (30 mL/h) and reduced at 600 °C for 3 hrs. under a hydrogen atmosphere (30 mL/h). The as-prepared catalyst was denoted as SiO_2/Zr-TEDTA. The SiO_2/Zr and SiO_2 without an EDTA template-assisted were also prepared.

3.2. Preparation of SiO_2/Zr Using EDTA Chelated-Assisted

In this procedure, the Zr precursor with the chelating agent is reacted by forming a complex bond. Briefly, ethanol (50 mL) was mixed with TEOS (25 mL) and stirred for 15 min at RT. Next, the solution containing $ZrOCl_2.8H_2O$ (2.578 g) and sodium EDTA (10%, 20 mL) was mixed with the as-prepared previous solution and stirred for 3 hrs. Afterward, the ammonium hydroxide solution (28%, 2 mL) was gradually added. The gel was left at RT for 30 min and subsequently dried in the oven at 85 °C for 24 hrs. The dried powder was later calcined in the muffle furnace at 850 °C for 3 hrs. under an oxygen atmosphere (30 mL/h). The SiO_2/ZrO_2-EDTA was washed until the pH reached 7. The solution was later heated to evaporate the water and subsequently dried at 120 °C for 24 h. The powder was later calcined at 850 °C for 3 hrs. under an oxygen atmosphere (30 mL/h) and reduced at 600 °C for 3 hrs. under a hydrogen atmosphere (30 mL/h). The as-prepared catalyst was denoted as SiO_2/Zr-CEDTA.

3.3. Characterization of Catalyst

The particle sizes of the catalysts (ranging from 0.01 μm to 5000 μm) were analyzed using Horiba Partica LA-960 equipped with a static light scattering method. The diffractograms of catalysts were assessed using a Rigaku SmartLab X-ray diffractometer. SEM-EDX mapping analysis was employed using JSM-IT200. The functional groups of catalysts

were investigated using Shimadzu FT1R-8201PC Infrared Spectrophotometer. The textural features of catalysts were evaluated using N_2 physorptions by NOVA Quantachrome. The total and surface acidity were determined using the gravimetric method with pyridine and ammonia as a probe [65], respectively, whereas the pore acidity was calculated using the subtraction of total acidity with surface acidity. The pyridine-adsorbed catalysts were also analyzed using FTIR.

3.4. Catalytic Hydrocracking Test

Catalytic hydrocracking was carried out in a continuous system micro-cylindrical reactor with an inner diameter of 2.5 cm, a length of 40 cm, and a capacity of 196.43 cm^3 [66]. Prior to the hydrocracking process, the reactor is saturated with hydrogen gas. CPO feed (38% of palmitic acid and 45.16% of oleic acid) is injected using a syringe pump into the reactor with a feed flow rate of 20 mL/h. 0.5 g of catalyst was employed, and the hydrocracking was conducted at 500 °C for 1 hr. with an H_2 flow rate of 30 mL/h. The product was then analyzed using GCMS. The product was then analyzed using GCMS (Thermo Scientific (Waltham, MA, USA)), equipped with TG-5MS columns. The products analysis was calculated according to the Equations (1)–(6):

$$\beta_L\ (\%.wt) = \frac{\alpha_L}{\alpha_F} \times 100\% \quad (1)$$

$$\beta_R\ (\%.wt) = \frac{\alpha_R}{\alpha_F} \times 100\% \quad (2)$$

$$\beta_C\ (\%.wt) = \frac{\alpha_C}{\alpha_F} \times 100\% \quad (3)$$

$$Y_G\ (\%.wt) = 100\% - (\beta_L + \beta_R + \beta_C)\%.wt \quad (4)$$

$$S_L\ (\%) = \frac{\%\ \text{GCMS}\ C_X - C_Y\ \text{fraction area}}{\%\ \text{GCMS total area}} \times 100\% \quad (5)$$

$$C_T(\%.wt) = \frac{\alpha_L - \alpha_R}{\alpha_F} \times 100\% \quad (6)$$

where β_L, β_R, β_C, and β_G are liquid, residue, coke, and gas yield, respectively, whereas S_L and C_T are the biofuel product selectivity and the total conversion, respectively. α_L is the weight of liquid, α_R is the weight of residue, α_C is the coke, and α_F is the weight of the feed. To investigate the stability of the catalyst towards CPO conversion, the spent catalyst was washed with hexane. The catalyst was dried at 105 °C for 1 hr., and subsequently calcinated and followed the reduction, as the same method with the fresh catalyst.

4. Conclusions

The preparation of SiO_2/Zr with different methods, i.e., chelate and template-assisted methods, was successfully conducted. These catalysts were employed for the crude palm oil (CPO) conversion to biofuels via hydrocracking. Different preparation revealed different physicochemical properties of catalysts, leading to different catalytic activities towards the CPO hydrocracking process. Among the catalysts evaluated, SiO_2/Zr-CEDTA showed the highest performance towards the CPO hydrocracking. This catalyst was able to attain a CPO conversion of 87.73% with a liquid yield of 66.29%.wt. The highest selectivity towards bio-jet was achieved up to 41.77%, followed by bio-diesel (31.43%) and bio-gasoline (26.80%). The SiO_2/Zr-CEDTE provided sufficient stability toward CPO conversion compared with SiO_2/Zr-TEDTA, as indicated by only an 11% decrease in the catalyst performance of CPO conversion after three runs.

Author Contributions: Conceptualization, H.H.; methodology, H.H.; validation, H.H.; formal analysis, Z.F., and F.H.; investigation, W.R.A., and S.J.A.; resources, H.H.; data curation, H.H., W.R.A.; writing—original draft preparation, W.R.A.; writing—review and editing, H.H.; Z.Z. and N.T.M.; visualization, R.M., and M.A.M.; supervision, H.H.; funding acquisition, H.H. All authors have read and agreed to the published version of the manuscript.

Funding: This research was funded by DRPM Ministry of Education, Culture, Research and Technology, Indonesia PDUPT Research grant SPPK No. 245/E5/PG.02.00.PT/2022 (as Research Contract Number: 0214/UN9.3.1/PL/2022).

Data Availability Statement: The data will be available at the request of the corresponding author.

Acknowledgments: This research was funded by DRPM Ministry of Education, Culture, Research and Technology, Indonesia PDUPT Research grant SPPK No. 245/E5/PG.02.00.PT/2022 (as Research Contract Number: 0214/UN9.3.1/PL/2022). The authors thank Badan Riset dan Inovasi Nasional (BRIN) for supplying the catalyst characterization instruments.

Conflicts of Interest: The authors declare no conflict of interest.

References

1. Rajesh, K.; Natarajan, M.P.; Devan, P.K.; Ponnuvel, S. Coconut Fatty Acid Distillate as Novel Feedstock for Biodiesel Production and Its Characterization as a Fuel for Diesel Engine. *Renew. Energy* **2021**, *164*, 1424–1435. https://doi.org/10.1016/j.renene.2020.10.082.
2. Sari, E.P.; Wijaya, K.; Trisunaryanti, W.; Syoufian, A.; Hasanudin, H.; Saputri, W.D. The Effective Combination of Zirconia Superacid and Zirconia-Impregnated CaO in Biodiesel Manufacturing: Utilization of Used Coconut Cooking Oil (UCCO). *Int. J. Energy Environ. Eng.* **2022**, *13*, 967–978. https://doi.org/10.1007/s40095-021-00439-4.
3. Mahdi, H.I.; Bazargan, A.; McKay, G.; Azelee, N.I.W.; Meili, L. Catalytic Deoxygenation of Palm Oil and Its Residue in Green Diesel Production: A Current Technological Review. *Chem. Eng. Res. Des.* **2021**, *174*, 158–187. https://doi.org/10.1016/j.cherd.2021.07.009.
4. Hassan, S.N.; Sani, Y.M.; Abdul Aziz, A.R.; Sulaiman, N.M.N.; Daud, W.M.A.W. Biogasoline: An out-of-the-Box Solution to the Food-for-Fuel and Land-Use Competitions. *Energy Convers. Manag.* **2015**, *89*, 349–367. https://doi.org/10.1016/j.enconman.2014.09.050.
5. Istadi, I.; Riyanto, T.; Buchori, L.; Anggoro, D.D.; Pakpahan, A.W.S.; Pakpahan, A.J. Biofuels Production from Catalytic Cracking of Palm Oil Using Modified Hy Zeolite Catalysts over a Continuous Fixed Bed Catalytic Reactor. *Int. J. Renew. Energy Dev.* **2021**, *10*, 149–156. https://doi.org/10.14710/ijred.2021.33281.
6. Melo-Banda, J.A. Catalytic Hydrocracking of Vegetable Oil for Agrofuels Production Using Ni-Mo, Ni-W, Pt and TFA Catalysts Supported on SBA-15. *Catal. Today* **2011**, *166*, 102–110. https://doi.org/10.1016/j.cattod.2011.01.026.
7. Hasanudin, H.; Asri, W.R.; Said, M.; Hidayati, P.T.; Purwaningrum, W.; Novia, N.; Wijaya, K. Hydrocracking Optimization of Palm Oil to Bio-Gasoline and Bio-Aviation Fuels Using Molybdenum Nitride-Bentonite Catalyst. *RSC Adv.* **2022**, *12*, 16431–16443. https://doi.org/10.1039/D2RA02438A.
8. Scaldaferri, C.A.; Pasa, V.M.D. Production of Jet Fuel and Green Diesel Range Biohydrocarbons by Hydroprocessing of Soybean Oil over Niobium Phosphate Catalyst. *Fuel* **2019**, *245*, 458–466. https://doi.org/10.1016/j.fuel.2019.01.179.
9. Ameen, M.; Azizan, M.T.; Yusup, S.; Ramli, A.; Yasir, M. Catalytic Hydrodeoxygenation of Triglycerides: An Approach to Clean Diesel Fuel Production. *Renew. Sustain. Energy Rev.* **2017**, *80*, 1072–1088. https://doi.org/10.1016/j.rser.2017.05.268.
10. Arun, N.; Sharma, R.V.; Dalai, A.K. Green Diesel Synthesis by Hydrodeoxygenation of Bio-Based Feedstocks: Strategies for Catalyst Design and Development. *Renew. Sustain. Energy Rev.* **2015**, *48*, 240–255. https://doi.org/10.1016/j.rser.2015.03.074.
11. Wang, S.; Guo, Z.; Cai, Q.; Guo, L. Catalytic Conversion of Carboxylic Acids in Bio-Oil for Liquid Hydrocarbons Production. *Biomass Bioenergy* **2012**, *45*, 138–143. https://doi.org/10.1016/j.biombioe.2012.05.023.
12. Hasanudin, H.; Asri, W.R.; Zulaikha, I.S.; Ayu, C.; Rachmat, A.; Riyanti, F.; Hadiah, F.; Zainul, R.; Maryana, R. Hydrocracking of Crude Palm Oil to a Biofuel Using Zirconium Nitride and Zirconium Phosphide-Modified Bentonite. *RSC Adv.* **2022**, *12*, 21916–21925. https://doi.org/10.1039/d2ra03941a.
13. Srihanun, N.; Dujjanutat, P.; Muanruksa, P.; Kaewekannetra, P. Biofuels of Green Diesel– Kerosene–Gasoline Production from Palm Oil : Effect of Palladium Cooperated with Second Metal on Hydrocracking Reaction. *Catalysts* **2020**, *10*, 241. https://doi.org/10.3390/catal10020241.
14. Liu, Y.; Murata, K.; Inaba, M. Hydrocracking of Algae Oil to Aviation Fuel-Ranged Hydrocarbons over NiMo-Supported Catalysts. *Catal. Today* **2019**, *332*, 115–121. https://doi.org/10.1016/j.cattod.2018.07.047.
15. Rasyid, R.; Malik, R.; Kusuma, H.S.; Roesyadi, A.; Mahfud, M. Triglycerides Hydrocracking Reaction of Nyamplung Oil with Non-Sulfided CoMo/γ-Al2O3 Catalysts. *Bull. Chem. React. Eng. Catal.* **2018**, *13*, 196–203. https://doi.org/10.9767/bcrec.13.2.734.196-203.
16. Li, T.; Cheng, J.; Huang, R.; Yang, W.; Zhou, J.; Cen, K. Hydrocracking of Palm Oil to Jet Biofuel over Different Zeolites. *Int. J. Hydrog. Energy* **2016**, *41*, 21883–21887. https://doi.org/10.1016/j.ijhydene.2016.09.013.

17. Ishihara, A.; Fukui, N.; Nasu, H.; Hashimoto, T. Hydrocracking of Soybean Oil Using Zeolite-Alumina Composite Supported NiMo Catalysts. *Fuel* **2014**, *134*, 611–617. https://doi.org/10.1016/j.fuel.2014.06.004.
18. Anand, M.; Farooqui, S.A.; Kumar, R.; Joshi, R.; Kumar, R.; Sibi, M.G.; Singh, H.; Sinha, A.K. Optimizing Renewable Oil Hydrocracking Conditions for Aviation Bio-Kerosene Production. *Fuel Process. Technol.* **2016**, *151*, 50–58. https://doi.org/10.1016/j.fuproc.2016.05.028.
19. Zandonai, C.H.; Yassue-Cordeiro, P.H.; Castellã-Pergher, S.B.; Scaliante, M.H.N.O.; Fernandes-Machado, N.R.C. Production of Petroleum-like Synthetic Fuel by Hydrocracking of Crude Soybean Oil over ZSM5 Zeolite-Improvement of Catalyst Lifetime by Ion Exchange. *Fuel* **2016**, *172*, 228–237. https://doi.org/10.1016/j.fuel.2015.12.059.
20. Schmidt, J.; De Rosa, M. Certified Palm Oil Reduces Greenhouse Gas Emissions Compared to Non-Certified. *J. Clean. Prod.* **2020**, *277*, 124045. https://doi.org/10.1016/j.jclepro.2020.124045.
21. Kuss, V.V.; Kuss, A.V.; Da Rosa, R.G.; Aranda, D.A.G.; Cruz, Y.R. Potential of Biodiesel Production from Palm Oil at Brazilian Amazon. *Renew. Sustain. Energy Rev.* **2015**, *50*, 1013–1020. https://doi.org/10.1016/j.rser.2015.05.055.
22. Purnomo, H.; Okarda, B.; Dermawan, A.; Ilham, Q.P.; Pacheco, P.; Nurfatriani, F.; Suhendang, E. Reconciling Oil Palm Economic Development and Environmental Conservation in Indonesia: A Value Chain Dynamic Approach. *For. Policy Econ.* **2020**, *111*, 102089. https://doi.org/10.1016/j.forpol.2020.102089.
23. Istadi, I.; Riyanto, T.; Khofiyanida, E.; Buchori, L.; Anggoro, D.D.; Sumantri, I.; Putro, B.H.S.; Firnanda, A.S. Low-Oxygenated Biofuels Production from Palm Oil through Hydrocracking Process Using the Enhanced Spent RFCC Catalysts. *Bioresour. Technol. Rep.* **2021**, *14*, 100677. https://doi.org/10.1016/j.biteb.2021.100677.
24. Šimáček, P.; Kubička, D. Hydrocracking of Petroleum Vacuum Distillate Containing Rapeseed Oil: Evaluation of Diesel Fuel. *Fuel* **2010**, *89*, 1508–1513. https://doi.org/10.1016/j.fuel.2009.09.029.
25. Li, J.; Fang, X.; Bian, J.; Guo, Y.; Li, C. Microalgae Hydrothermal Liquefaction and Derived Biocrude Upgrading with Modified SBA-15 Catalysts. *Bioresour. Technol.* **2018**, *266*, 541–547. https://doi.org/10.1016/j.biortech.2018.07.008.
26. Nasseri, M.A.; Sadeghzadeh, M. Multi-Component Reaction on Free Nano-SiO2 Catalyst: Excellent Reactivity Combined with Facile Catalyst Recovery and Recyclability. *J. Chem. Sci.* **2013**, *125*, 537–544. https://doi.org/10.1007/s12039-013-0403-0.
27. Yao, L.; Shi, J.; Xu, H.; Shen, W.; Hu, C. Low-Temperature CO_2 Reforming of Methane on Zr-Promoted Ni/SiO2 Catalyst. *Fuel Process. Technol.* **2016**, *144*, 1–7. https://doi.org/10.1016/j.fuproc.2015.12.009.
28. Tu, Y.J.; Chen, Y.W. Effects of Alkali Metal Oxide Additives on Cu/SiO_2 Catalyst in the Dehydrogenation of Ethanol. *Ind. Eng. Chem. Res.* **2001**, *40*, 5889–5893. https://doi.org/10.1021/ie010272q.
29. Lomate, S.; Sultana, A.; Fujitani, T. Effect of SiO_2 Support Properties on the Performance of Cu-SiO_2 Catalysts for the Hydrogenation of Levulinic Acid to Gamma Valerolactone Using Formic Acid as a Hydrogen Source. *Catal. Sci. Technol.* **2017**, *7*, 3073–3083. https://doi.org/10.1039/c7cy00902j.
30. Shu, R.; Xu, Y.; Chen, P.; Ma, L.; Zhang, Q.; Zhou, L.; Wang, C. Mild Hydrogenation of Lignin Depolymerization Products over Ni/SiO2 Catalyst. *Energy Fuels* **2017**, *31*, 7208–7213. https://doi.org/10.1021/acs.energyfuels.7b00934.
31. Wu, C.; Williams, P.T. A Novel Nano-Ni/SiO2 Catalyst for Hydrogen Production from Steam Reforming of Ethanol. *Environ. Sci. Technol.* **2010**, *44*, 5993–5998. https://doi.org/10.1021/es100912w.
32. Giniyatova, S.; Dauletbekova, A.; Baimukhanov, Z.; Vlasukova, L.; Akilbekov, A.; Usseinov, A.; Kozlovskiy, A.; Akylbekova, A.; Seitbayev, A.; Karipbayev, Z. Structure, Electrical Properties and Luminescence of ZnO Nanocrystals Deposited in SiO2/Si Track Templates. *Radiat. Meas.* **2019**, *125*, 52–56. https://doi.org/10.1016/j.radmeas.2019.04.001.
33. Wang, H.; Chen, Z.; Chen, D.; Yu, Q.; Yang, W.; Zhou, J.; Wu, S. Facile, Template-Free Synthesis of Macroporous SiO2 as Catalyst Support towards Highly Enhanced Catalytic Performance for Soot Combustion. *Chem. Eng. J.* **2019**, *375*, 121958. https://doi.org/10.1016/j.cej.2019.121958.
34. Zhu, Q.; Zhang, H.; Zhang, S.; Wang, G.; Zhu, X.; Li, C. Dehydrogenation of Isobutane over a Ni-P/SiO2 Catalyst: Effect of P Addition. *Ind. Eng. Chem. Res.* **2019**, *58*, 7834–7843. https://doi.org/10.1021/acs.iecr.9b00032.
35. Mashkin, M.; Tedeeva, M.; Fedorova, A.; Vasiliev, A.; Egorov, A.; Pribytkov, P.; Kalmykov, K.; Kapustin, G.; Morozov, I.; Kustov, L.; et al. CrOx/SiO_2 Mesoporous Catalysts Prepared Using Beta-Cyclodextrin as a Template and Their Catalytic Properties in Propane Oxidative Dehydrogenation in the Presence of Carbon Dioxide. *Microporous Mesoporous Mater.* **2022**, *338*, 111967. https://doi.org/10.1016/j.micromeso.2022.111967.
36. Vasiliadou, E.S.; Lemonidou, A.A. Parameters Affecting the Formation of 1,2-Propanediol from Glycerol over Ru/SiO_2 Catalyst. *Org. Process Res. Dev.* **2011**, *15*, 925–931. https://doi.org/10.1021/op2000173.
37. Peng, L.; Zhao, Y.; Yang, T.; Tong, Z.; Tang, Z.; Orita, A.; Qiu, R. Zirconium-Based Catalysts in Organic Synthesis. *Top. Curr. Chem.* **2022**, *380*, 41. https://doi.org/10.1007/s41061-022-00396-4.
38. Liu, Y.; Liu, X.; Li, M.; Meng, Y.; Li, J.; Zhang, Z.; Zhang, H. Recyclable Zr/Hf-Containing Acid-Base Bifunctional Catalysts for Hydrogen Transfer Upgrading of Biofuranics: A Review. *Front. Chem.* **2021**, *9*, 1090. https://doi.org/10.3389/fchem.2021.812331.
39. Zhao, Y.; Sohn, H.; Hu, B.; Niklas, J.; Poluektov, O.G.; Tian, J.; Delferro, M.; Hock, A.S. Zirconium Modification Promotes Catalytic Activity of a Single-Site Cobalt Heterogeneous Catalyst for Propane Dehydrogenation. *ACS Omega* **2018**, *3*, 11117–11127. https://doi.org/10.1021/acsomega.8b00862.
40. Zhang, Q.; Long, K.; Wang, J.; Zhang, T.; Song, Z.; Lin, Q. A Novel Promoting Effect of Chelating Ligand on the Dispersion of Ni Species over Ni/SBA-15 Catalyst for Dry Reforming of Methane. *Int. J. Hydrog. Energy* **2017**, *42*, 14103–14114. https://doi.org/10.1016/j.ijhydene.2017.04.090.

41. Ren, H.P.; Hao, Q.Q.; Ding, S.Y.; Zhao, Y.Z.; Zhu, M.; Tian, S.P.; Ma, Q.; Song, W.Q.; Miao, Z.; Liu, Z.T. A High-Performance Ni/SiO2 Prepared by the Complexed-Impregnation Method with Citric Acid for Carbon Dioxide Reforming of Methane. *Ind. Eng. Chem. Res.* **2018**, *57*, 16257–16263. https://doi.org/10.1021/acs.iecr.8b03897.
42. Bian, Z.; Xin, Z.; Meng, X.; Tao, M.; Lv, Y.H.; Gu, J. Effect of Citric Acid on the Synthesis of CO Methanation Catalysts with High Activity and Excellent Stability. *Ind. Eng. Chem. Res.* **2017**, *56*, 2383–2392. https://doi.org/10.1021/acs.iecr.6b04027.
43. Li, W.; Zhao, Z.; Ding, F.; Guo, X.; Wang, G. Syngas Production via Steam-CO_2 Dual Reforming of Methane over LA-Ni/ZrO2 Catalyst Prepared by l -Arginine Ligand-Assisted Strategy: Enhanced Activity and Stability. *ACS Sustain. Chem. Eng.* **2015**, *3*, 3461–3476. https://doi.org/10.1021/acssuschemeng.5b01277.
44. Ran, R.; Guo, Y.; Zheng, Y.; Wang, K.; Shao, Z. Well-Crystallized Mesoporous Samaria-Doped Ceria from EDTA-Citrate Complexing Process with in Situ Created NiO as Recyclable Template. *J. Alloy. Compd.* **2010**, *491*, 271–277. https://doi.org/10.1016/j.jallcom.2009.10.129.
45. Rodríguez-González, V.; Marceau, E.; Beaunier, P.; Che, M.; Train, C. Stabilization of Hexagonal Close-Packed Metallic Nickel for Alumina-Supported Systems Prepared from Ni(II) Glycinate. *J. Solid State Chem.* **2007**, *180*, 22–30. https://doi.org/10.1016/j.jssc.2006.09.015.
46. Kaplin, I.Y.; Lokteva, E.S.; Golubina, E.V.; Lunin, V.V. Template Synthesis of Porous Ceria-Based Catalysts for Environmental Application. *Molecules* **2020**, *25*, 4242. https://doi.org/10.3390/molecules25184242.
47. Purwaningsih, H.; Ervianto, Y.; Pratiwi, V.M.; Susanti, D.; Purniawan, A. Effect of Cetyl Trimethyl Ammonium Bromide as Template of Mesoporous Silica MCM-41 from Rice Husk by Sol-Gel Method. *IOP Conf. Ser. Mater. Sci. Eng.* **2019**, *515*, 012051. https://doi.org/10.1088/1757-899X/515/1/012051.
48. Rubab, R.; Ali, S.; Rehman, A.U.; Khan, S.A.; Khan, A.M. Templated Synthesis of NiO/SiO_2 Nanocomposite for Dye Removal Applications: Adsorption Kinetics and Thermodynamic Properties. *Colloids Surf. A Physicochem. Eng. Asp.* **2021**, *615*, 126253. https://doi.org/10.1016/j.colsurfa.2021.126253.
49. Koizumi, N.; Ibi, Y.; Hongo, D.; Hamabe, Y.; Suzuki, S.; Hayasaka, Y.; Shindo, T.; Yamada, M. Mechanistic Aspects of the Role of Chelating Agents in Enhancing Fischer-Tropsch Synthesis Activity of Co/SiO_2 Catalyst: Importance of Specific Interaction of Co with Chelate Complex during Calcination. *J. Catal.* **2012**, *289*, 151–163. https://doi.org/10.1016/j.jcat.2012.02.003.
50. Wijaya, K.; Malau, L.L.M.; Utami, M.; Mulijani, S.; Patah, A.; Wibowo, A.C.; Chandrasekaran, M.; Rajabathar, J.R.; Al-Lohedan, H.A. Synthesis, Characterizations and Catalysis of Sulfated Silica and Nickel Modified Silica Catalysts for Diethyl Ether (DEE) Production from Ethanol towards Renewable Energy Applications. *Catalysts* **2021**, *11*, 1511. https://doi.org/10.3390/catal11121511.
51. Aneu, A.; Wijaya, K.; Syoufian, A. Silica-Based Solid Acid Catalyst with Different Concentration of H_2SO_4 and Calcination Temperature: Preparation and Characterization. *Silicon* **2021**, *13*, 2265–2270. https://doi.org/10.1007/s12633-020-00741-6.
52. Kumar, S.; Bhunia, S.; Ojha, A.K. Effect of Calcination Temperature on Phase Transformation, Structural and Optical Properties of Sol-Gel Derived ZrO_2 Nanostructures. *Phys. E Low-Dimens. Syst. Nanostructures* **2015**, *66*, 74–80. https://doi.org/10.1016/j.physe.2014.09.007.
53. Rauta, P.R.; Manivasakan, P.; Rajendran, V.; Sahu, B.B.; Panda, B.K.; Mohapatra, P. Phase Transformation of ZrO_2 Nanoparticles Produced from Zircon. *Phase Transit.* **2012**, *85*, 13–26. https://doi.org/10.1080/01411594.2011.619698.
54. Utami, M.; Safitri, R.; Fajar Pradipta, M.; Wijaya, K.; Woong Chang, S.; Ravindran, B.; Ovi, D.; Rajabathar, J.R.; Poudineh, N.; Moonsamy Gengan, R. Enhanced Catalytic Conversion of Palm Oil into Biofuels by Cr-Incorporated Sulphated Zirconia. *Mater. Lett.* **2022**, *309*, 131472. https://doi.org/10.1016/j.matlet.2021.131472.
55. Wijaya, K.; Nadia, A.; Dinana, A.; Pratiwi, A.F.; Tikoalu, A.D.; Wibowo, A.C. Catalytic Hydrocracking of Fresh and Waste Frying Oil over Ni-and Mo-Based Catalysts Supported on Sulfated Silica for Biogasoline Production. *Catalysts* **2021**, *11*, 1150. https://doi.org/10.3390/catal11101150.
56. Nadia, A.; Wijaya, K.; Falah, I.I.; Sudiono, S.; Budiman, A. Self-Regeneration of Monodisperse Hierarchical Porous NiMo/Silica Catalyst Induced by $NaHCO_3$ for Biofuel Production. *Waste Biomass Valorization* **2021**, *13*, 2335–2347. https://doi.org/10.1007/s12649-021-01634-4.
57. Tran, T.N.; Pham, T.V.A.; Le, M.L.P.; Nguyen, T.P.T.; Tran, V.M. Synthesis of Amorphous Silica and Sulfonic Acid Functionalized Silica Used as Reinforced Phase for Polymer Electrolyte Membrane. *Adv. Nat. Sci. Nanosci. Nanotechnol.* **2013**, *4*, 045007. https://doi.org/10.1088/2043-6262/4/4/045007.
58. Gobara, H.M.; Hassan, S.A.; Betiha, M.A. The Interaction Characteristics Controlling Dispersion Mode-Catalytic Functionality Relationship of Silica–Modified Montmorillonite-Anchored Ni Nanoparticles in Petrochemical Processes. *Mater. Chem. Phys.* **2016**, *181*, 476–486. https://doi.org/10.1016/j.matchemphys.2016.06.084.
59. Badoga, S.; Mouli, K.C.; Soni, K.K.; Dalai, A.K.; Adjaye, J. Beneficial Influence of EDTA on the Structure and Catalytic Properties of Sulfided NiMo/SBA-15 Catalysts for Hydrotreating of Light Gas Oil. *Appl. Catal. B Environ.* **2012**, *125*, 67–84. https://doi.org/10.1016/j.apcatb.2012.05.015.
60. Zaki, T.; Mukhtarova, G.S.; Al-Sabagh, A.M.; Soliman, F.S.; Betiha, M.A.; Mahmoud, T.; Abd El-Raouf, M.; Afandiyeva, N.K.; Alizade, A.; Hasanova, A.B.; et al. Slurry-Phase Catalytic Hydrocracking of Mazut (Heavy Residual Fuel Oil) Using Ni-Bentonite. *Pet. Sci. Technol.* **2018**, *36*, 1559–1567. https://doi.org/10.1080/10916466.2018.1490762.
61. Hasanudin, H.; Asri, W.R.; Andini, L.; Riyanti, F.; Mara, A.; Hadiah, F.; Fanani, Z. Enhanced Isopropyl Alcohol Conversion over Acidic Nickel Phosphate-Supported Zeolite Catalysts. *ACS Omega* **2022**, *7*, 38923–38932. https://doi.org/10.1021/acsomega.2c04647.

62. Hasanudin, H.; Asri, W.R.; Putri, Q.U.; Fanani, Z.; Agustina, T.E.; Wijaya, K. Montmorillonite-Zirconium Phosphate Catalysts for Methanol Dehydration. *Iran. J. Catal.* **2022**, *12*, 389–397. https://doi.org/10.30495/IJC.2022.1960655.1942.
63. Wijaya, K.; Kurniawan, M.A.; Saputri, W.D.; Trisunaryanti, W.; Mirzan, M.; Hariani, P.L.; Tikoalu, A.D. Synthesis of Nickel Catalyst Supported on ZrO_2/SO_4 pillared Bentonite and Its Application for Conversion of Coconut Oil into Gasoline via Hydrocracking Process. *J. Environ. Chem. Eng.* **2021**, *9*, 105399. https://doi.org/10.1016/j.jece.2021.105399.
64. Alisha, G.D.; Trisunaryanti, W.; Syoufian, A. Hydrocracking of Waste Palm Cooking Oil into Hydrocarbon Compounds over Mo Catalyst Impregnated on SBA-15. *Silicon* **2022**, *14*, 2309–2315. https://doi.org/10.1007/s12633-021-01035-1.
65. Aziz, I.T.A.; Saputri, W.D.; Trisunaryanti, W.; Sudiono, S.; Syoufian, A.; Budiman, A.; Wijaya, K. Synthesis of Nickel-Loaded Sulfated Zirconia Catalyst and Its Application for Converting Used Palm Cooking Oil to Gasoline via Hydrocracking Process. *Period. Polytech. Chem. Eng.* **2022**, *66*, 101–113. https://doi.org/10.3311/PPch.18209.
66. Hasanudin, H.; Rachmat, A.; Said, M.; Wijaya, K. Kinetic Model of Crude Palm Oil Hydrocracking over Ni/Mo ZrO_2 –Pillared Bentonite Catalyst. *Period. Polytech. Chem. Eng.* **2020**, *64*, 238–247. https://doi.org/10.3311/PPch.14765.